Measurement and Analysis of Power Losses in Sintered Cores for Power Electronic Devices in Renewable Energy Systems

Pawel Lasek[1]
Department of Power Electronics,
Electrical Drives and Robotics,
Silesian University of Technology,
Gliwice 44-100, Poland
e-mail: pawel.lasek@polsl.pl

Mariusz Stepien
Department of Power Electronics,
Electrical Drives and Robotics,
Silesian University of Technology,
Gliwice 44-100, Poland
e-mail: mariusz.stepien@polsl.pl

Measurement of power losses in inductive devices in highly efficient power electronic systems is crucial for choosing appropriate components. A calorimetric method for measuring power losses below 10 W is presented in the following paper to decompose the inductive devices' power losses. A fully enclosed double-jacked calorimetric chamber is constructed to measure the temperature with digital temperature sensors TMP275, providing a resolution of 0.1 W/K. The finite element method is used with analytical calculation to estimate core and conduction losses to decompose power losses. Power losses are measured for an inductor with a 3C95 ferrite core and four types of windings, where three were made of wire with a different number of strands, whereas the fourth has been made using copper foil. All windings have similar cross-sectional areas for comparison.
[DOI: 10.1115/1.4052791]

Keywords: energy conversion systems, renewable energy, power electronics, calorimetry, inductors

Introduction

With an increasing number of renewable energy systems, global trends are focused on increasing electrical energy conversion efficiency with a simultaneous decrease in cost and dimensions of devices. This is usually achieved by operating at higher frequency ranges above 10 kHz. Ferromagnetic-based components are one of the major elements in power electronic devices where power losses, dimensions, and weight can be reduced. In renewable sources, such as photovoltaic panels or low power, domestic wind turbines power electronic devices are used to convert electrical energy. The ferromagnetic materials are used in inductive elements such as chokes and transformers. The primary consideration is picking the material for given operating conditions depending on the device, like in DC/DC or DC/AC converters [1,2]. The following papers' main objective is to analyze losses occurring in inductors using the calorimetric method, where cores are made of different materials, like ferrites suited for high-frequency currents. The power losses in these devices occur in both winding and core. However, measuring power losses in such devices is not an easy task since these have high Q-factor due to relatively high inductance and very low resistance. The losses cannot be measured using DC current due to additional effects during AC operation, such as skin and proximity effects and core losses that are not generated in the DC field.

It is expected that power losses in analyzed components are at the level of 10 W. The current waveforms through inductive components in most applications are sinusoidal with a high-frequency ripple as shown in Fig. 1(*a*) or triangular with DC bias in Fig. 1(*b*). The former is typical for DC/AC converters, whereas the latter for DC/DC converters like BUCK or BOOST. Both waveforms carry a spectra of higher-order harmonics, which are making power losses inherently difficult to analyze. When current and voltage waveforms can be analyzed using Fourier transform, the phase shift between every major harmonic would be nearly 90 deg. The phase shift would decrease only when the skin and proximity effects become significant, resulting in increased AC resistance, which is unwanted [2].

State of the Art

The calorimetric method poses an alternative to the electric-based measurement of power losses. Comparison between electrical and calorimetric measurements of inductive components shows higher accuracy of the latter, especially in soft-iron powder cores, especially in cores with relative magnetic permeability $\mu_r < 300$ [3]. The ferrite material 3C95 is an order of magnitude higher permeable to magnetic field $\mu_r \approx 5000$ [4] compared to soft iron powders [5]. So far, various such devices were built for high precision calorimetric measurement [6,7]. The use of a heat exchanges, where dissipated power is measured from liquid flow and temperature difference between inlet and outlet, allows for measurement of power losses of hundreds of watts [8]. Higher precision is obtained by using a double-jacket close type chamber [9] compared to single jacket chambers, due to confinement of heat in the inner chamber, whereas the outer chamber serves and insulation from the environment. The outer chamber can also serve as a reference when equipped with heaters to stabilize the temperature [9,10]. Calorimetric measurements are usually performed to reach thermal steady-state in the system, although it has been shown that estimation of generated power losses by observing temperatures in transient state results in good accuracy [11]. This can be done by having two identical chambers, one with the measured device and the second with a reference heat source controlled via a controller to match the temperature increase in the former. Performing measurement based on the transient state has two advantages: first, it is much quicker than measurement based on reaching steady-state, although less accurate; second, the measured power losses can be higher than nominal for the chamber, since temperature rise is lower than nominal. Besides power losses in inductive elements, also power losses in capacitors can be measured using the same system [12] or power electronic converters [1,7] with good precession, although some consideration regarding the operating temperature of other components, i.e., semiconductors, should be taken into account to avoid damage due to overheating.

[1]Corresponding author.

Contributed by the Advanced Energy Systems Division of ASME for publication in the Journal of Energy Resources Technology. Manuscript received March 31, 2021; final manuscript received October 18, 2021; published online November 12, 2021. Assoc. Editor: Tatiana Morosuk.

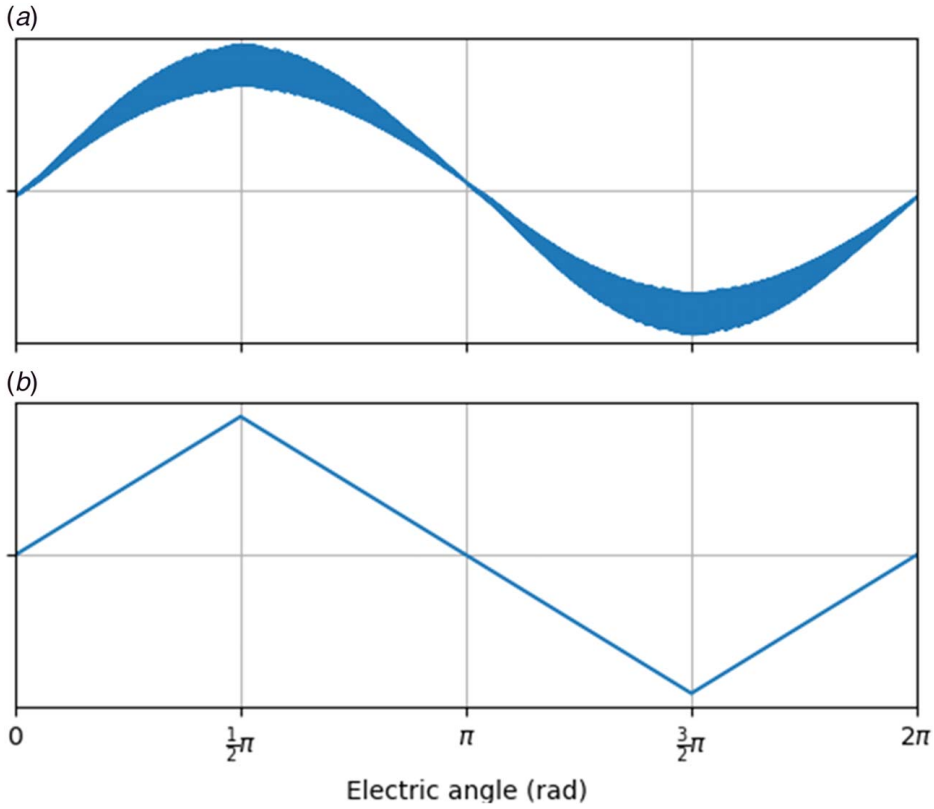

Fig. 1 Example waveforms typical for power electronic devices: (*a*) sinusoidal with high-frequency ripple and (*b*) triangular waveform

Calorimetric Measurement System

The setup of the chamber and sensor placement is shown in Fig. 2. Both chambers were made of white Styrofoam with thermal conductivity 0.040 W/mK. The outer chamber has inner dimensions of $500 \times 300 \times 285$ mm and 40 mm wall thickness, whereas the inner chamber has inner dimensions of $150 \times 150 \times 100$ mm with 30 mm wall thickness. The inner chamber was located in the very center of the outer chamber on Styrofoam stands to avoid direct contact with the bottom. The inductor has been placed on fiberglass PCB composite at an even distance to every wall.

Eight temperature sensors, TMP275, measure temperature on walls of the inner and outer chambers. Three sensors were placed on walls perpendicular to each other in both chambers. A higher amount of heat flux is expected to escape through the top of the calorimeter due to natural convection; therefore, sensor no. 6 was placed on the inner top wall of the inner chamber, sensor no. 3 on the outer chambers' inner top wall and sensor no. 1 on the top outer wall of the outer chamber. Multiple sensors were placed in each chamber to ensure that the temperature field is as homogenous inside as possible. The sensor no. 0 measured ambient temperature. As a heater, the Arcol HS50 15R J power resistor has been used with a low electrical resistance temperature coefficient.

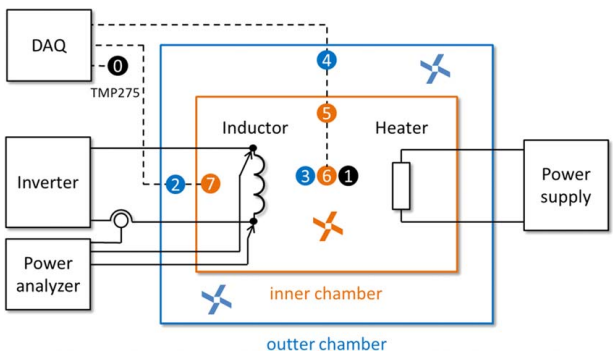

Fig. 2 Diagram of the system for calorimetric measurement

To measure the inductors' power losses, the Yokogawa WT5000 precision power analyzer had been connected using the four-wire method to the inductor in question. The inductors were powered from a custom-built inverter—a full-bridge single phase inverter capable of generating various waveforms with DC bias. The inductors were connected through 630×0.1 mm Litz wire to reduce additional losses and minimize potential heat sources during operation. To evenly distribute heat in both chambers, fans are required. A single fan was used for the internal, and two fans in the outer chamber. These fans have to operate constantly to force convection and spread air. The fans used in the setup were AAB Super Silent Fan 8 Pro due to relatively low power consumption. Each fan dissipates an additional 1.2 W of power at 12 V, which has to be taken into account.

Since both chambers have fans installed that dissipate heat continuously, it is necessary to consider those when calculating power losses during the measurement. The power generated inside the chamber dissipates through walls. In steady-state, the power losses generated inside the chamber can be calculated using Eq. (1).

$$\Delta P_{\text{tot inner}} = \frac{T_{\text{inner}} - T_{\text{amb}} - \Delta P_{\text{out}} R_{\text{th outer}}}{R_{\text{th inner}} + R_{\text{th outer}}} = \frac{\Delta T - \Delta P_{\text{out}} R_{\text{th outer}}}{R_{\text{th inner}} + R_{\text{th outer}}} \tag{1}$$

$$\Delta P_{\text{tot}} = \Delta P_{\text{tot inner}} - \Delta P_{\text{fan}} \tag{2}$$

The major disadvantage of using a fully closed double-jacket calorimetric chamber is the accumulation of heat in the chamber, which

results in increased temperature that might not reflect precisely the operating conditions of the measured devices. The devices would operate at lower temperatures in real-world applications, since the heat would most likely be removed from the system. However, the heat exchanger introduces another source of error. Therefore, in the proposed method, losses can be considered at the given temperature and scaled accordingly. For example, losses in ferrites can be scaled using a quadratic function with a minimum at around 90 °C according to Eq. (7). The resistivity of the windings changes linearly with temperature and will affect conduction losses. It also affects losses associated with skin and proximity effects and additional losses due to magnetomotive force (MMF) near the air gaps that can be related to the fringing effect. The local eddy current density in the wire depends on skin depth, which is temperature-dependent, and these effects do not scale linearly.

Measured Devices. The windings are usually made using different wire diameters and types, like solid copper wires or Litz wires. Which type is used usually depends on manufacturing and operational costs. Solid enameled copper wire is much cheaper than Litz wire, but results in increased losses during operation. On the other hand, the number and diameter of individual strands in Litz wire increase not only the cost but also the efficiency of the device. The compromise is found when the radius of a strand or wire is comparable with skin depth in Eq. (3). If the skin depth is higher or equal to the radius of the wire, it can be assumed that current density is uniform.

$$\delta = \sqrt{\frac{\varrho(T)}{\mu_0 \pi f}} \tag{3}$$

The resistivity of the conductor changes with temperature in Eq. (4) and affects the skin depth.

$$\varrho(T) = \varrho_{\text{ref}}[1 + \alpha_{\text{th}}(T - T_{\text{ref}})] \tag{4}$$

Three different wires have been chosen for windings with approximately similar cross-sectional areas: 2×1.5 mm, 35×0.355 mm and 400×0.1 mm as shown in Figs. 3(*a*)–3(*c*). The devices will be powered from an inverter with a 35 kHz voltage square wave, which will result in triangular current waveform shown in Fig. 1(*b*). This corresponds to 0.35 mm of skin depth at 23 °C for the first harmonic. All windings have a similar cross-sectional area and similar resistance of c.a. 20 mΩ with minor differences. Measured inductors have an inductance of 250 μH, which has been achieved by winding a coil with 24 turns on a pair of E65 3C95 ferrite cores with a 1 mm air gap. To compare effectiveness of different winding types, a coil has been wounded with a copper foil with an 100 μm of thickness and 34 mm of height with an insulating polyamide tape between each turn as shown in Fig. 3(*d*).

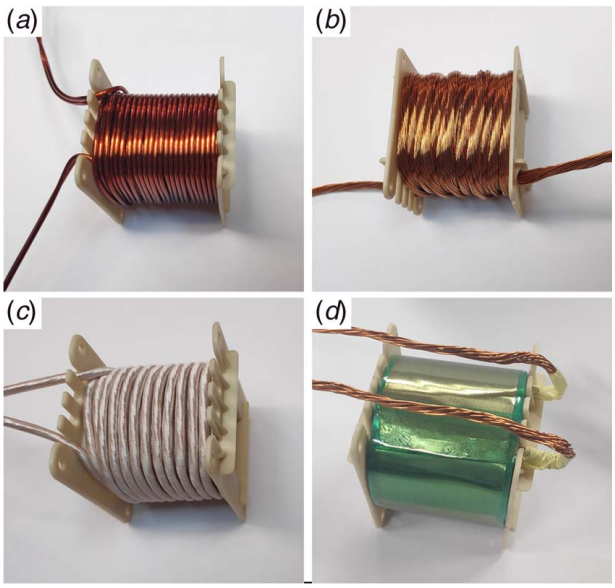

Fig. 3 Windings used in research (*a*) 2 × 1.5 mm, (*b*) 35 × 0.355 mm, (*c*) 400 × 0.1 mm, and (*d*) foil 0.1 × 34 mm

In some applications, foil is preferable due to the possibility of obtaining a high fill factor and better thermal conductivity of the winding compared to round wires. The main disadvantage of using foil-type winding is the high vulnerability to additional eddy current losses caused by the magnetic field acting perpendicular to the surface of the foil, i.e., due to the fringing effect of the stray magnetic field crossing the inductors' window. A copper winding is preferable to achieve high efficiency, but in high-voltage and low-current applications, aluminum can reduce overall costs. Some compromise in reducing power losses and achieving a high fill factor is possible by using Litz wire with a rectangular cross section, but that usually comes with a higher cost than foil winding.

Power Loss Decomposition

Major power losses in inductive components can be split between core and winding as shown in Eq. (5). In inductors, the ferromagnetic core losses are proportional to the peak value of current flowing through the coil. Known power loss models like General Steinmetz Equation (GSE) are based on monoharmonic waveforms. Another widely applicable model is the improved General Steinmetz Equation (iGSE) as in Eq. (6) or improved-improved GSE (i^2GSE), where losses can be calculated for arbitrary waveforms. To calculate power losses inside the core, a lumped magnetic circuit model can be used or finite element method (FEM) that takes into account the non-uniform distribution of magnetic flux inside the core, resulting in better loss estimation. If the current waveform has DC bias, the losses differ from those without it due to different operating points on the B-H curve of ferromagnetic material. If the current waveform has a constant component, the relaxation term must be considered, like in i^2GSE. To avoid the influence of these effects, only a triangular waveform without DC bias is considered in the following research [13–15]:

$$\Delta P_{\text{tot}} = \Delta P_{\text{Fe}} + \Delta P_{\text{Cu}} \tag{5}$$

$$\Delta P_{\text{Fe}} = V \frac{1}{T} \int_0^T k(T) \cdot \left(\frac{\mathrm{d}B(t)}{\mathrm{d}t} \right)^{\alpha} \cdot \Delta B^{\beta - \alpha} \mathrm{d}t \tag{6}$$

$$k(T) = C_2 T^2 + C_1 T + C_0 \tag{7}$$

Estimating power losses is more difficult due to the high-frequency current, resulting in skin effect and non-uniform current density distribution inside the wire. However, there are other phenomena like the proximity effect, since winding is composed of multiple strands and turns and additional currents induced via fringing close to the cores' air gaps. Both types of losses result in total winding losses. The skin and proximity effects can be taken into account by either measuring or calculating AC resistance at the given frequency. The AC resistance depends on frequency because of the reasons mentioned above and can be parametrized as some multiple of DC resistance. This results in conduction losses, and the remaining part ΔP_{add} should come from eddy currents induced from fringing effect as in Eq. (8). The total conduction losses cannot be measured without a magnetic core because this changes the distribution of the magnetic field acting on the winding [16].

$$\Delta P_{\text{Cu}} = \Delta P_{\text{cond}} + \Delta P_{\text{add}} \tag{8}$$

Calculating winding losses using FEM is a difficult task due to the necessity of simulating every strand individually, increasing the total number of elements to simulate all effects mentioned

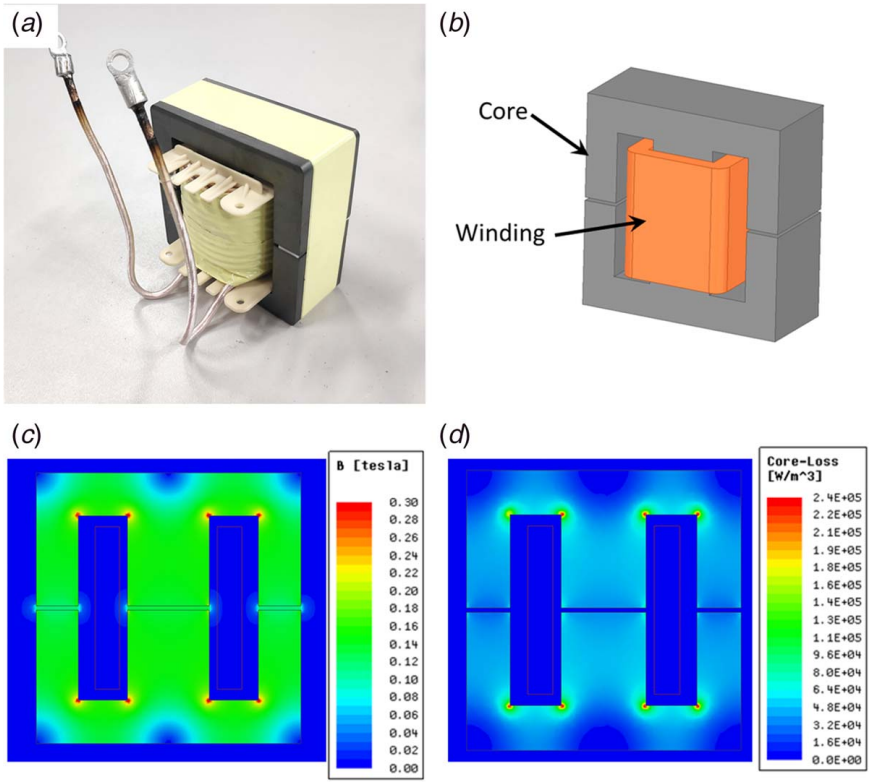

Fig. 4 FEM simulation: (*a*) assembled inductor to model, (*b*) geometry setup, (*c*) magnetic flux density distribution, and (*d*) core power loss distribution

previously. To simulate skin effect, at least three to five elements per radius of every wire are required, which increases the number of elements immensely, even in 2D models.

Finite Element Method Modeling of Inductors

If the waveform of magnetic flux inside the core is known, estimating power losses analytically using iGSE is possible, but methods such as the finite-element method allow for taking into account the field distribution inside the core. For a known distribution of current density, the magnetic vector potential can be calculated using $\mathbf{A}$ – formulation (Eq. (9)), from which magnetic flux density can be evaluated (10). The solution was obtained using FEM software with ANSYS ELECTRONICS.

$$\nabla \times \frac{1}{\mu} \nabla \times \mathbf{A} + \frac{1}{\varrho} \frac{\partial \mathbf{A}}{\partial t} = \mathbf{J} \tag{9}$$

$$\mathbf{B} = \nabla \times \mathbf{A} \tag{10}$$

The distribution of magnetic flux density inside the core is mostly uniform, with higher values around the corners as shown in Fig. 4(*c*). The magnetic flux density in the vicinity of the air gaps leaks out of the core due to fringing effect. This magnetic field results in additional losses due to induced eddy currents in windings nearby. The simulation results show that power loss distribution inside the core is homogeneous, as shown in Fig. 4(*d*).

Calculating winding losses with all effects taken into account using FEM is computationally demanding and has been omitted. The winding has been modeled as a homogenous solid as shown in Fig. 4(*b*) with a given current density and does not affect magnetic field distribution. Measured losses are split between winding and core losses. The mathematical model for loss estimation is derived for different types of waveforms and frequencies, as in Eq. (11). The following model is used for coupled FEM simulation to calculate power losses and temperature field for tested current waveforms.

$$\Delta P_{\mathrm{Cu}} = R_{\mathrm{AC}} I_{\mathrm{RMS}}^2 = (F_{\mathrm{R}} + G_{\mathrm{R}}) R_{\mathrm{DC}} I_{\mathrm{RMS}}^2 \tag{11}$$

The calculation of skin effect F_{R} and proximity effect G_{R} factors is based on Kelvin functions. The parameters take into account the number of strands of Litz wire, spacing, skin depth, and the total amount of winding conductors described in detail in Ref. [17].

Results and Discussion

The calorimetric chamber was calibrated for every inductor, since installing it into the chamber might result in the Styrofoam lid misalignment and, therefore, changing its parameters. Later, during

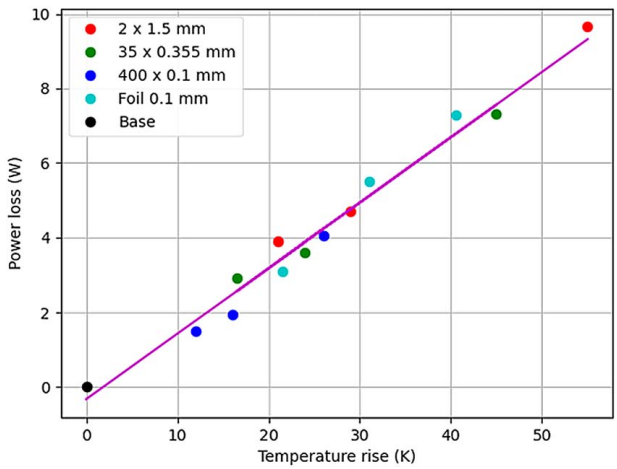

Fig. 5 Calibration characteristic of the calorimetric chamber

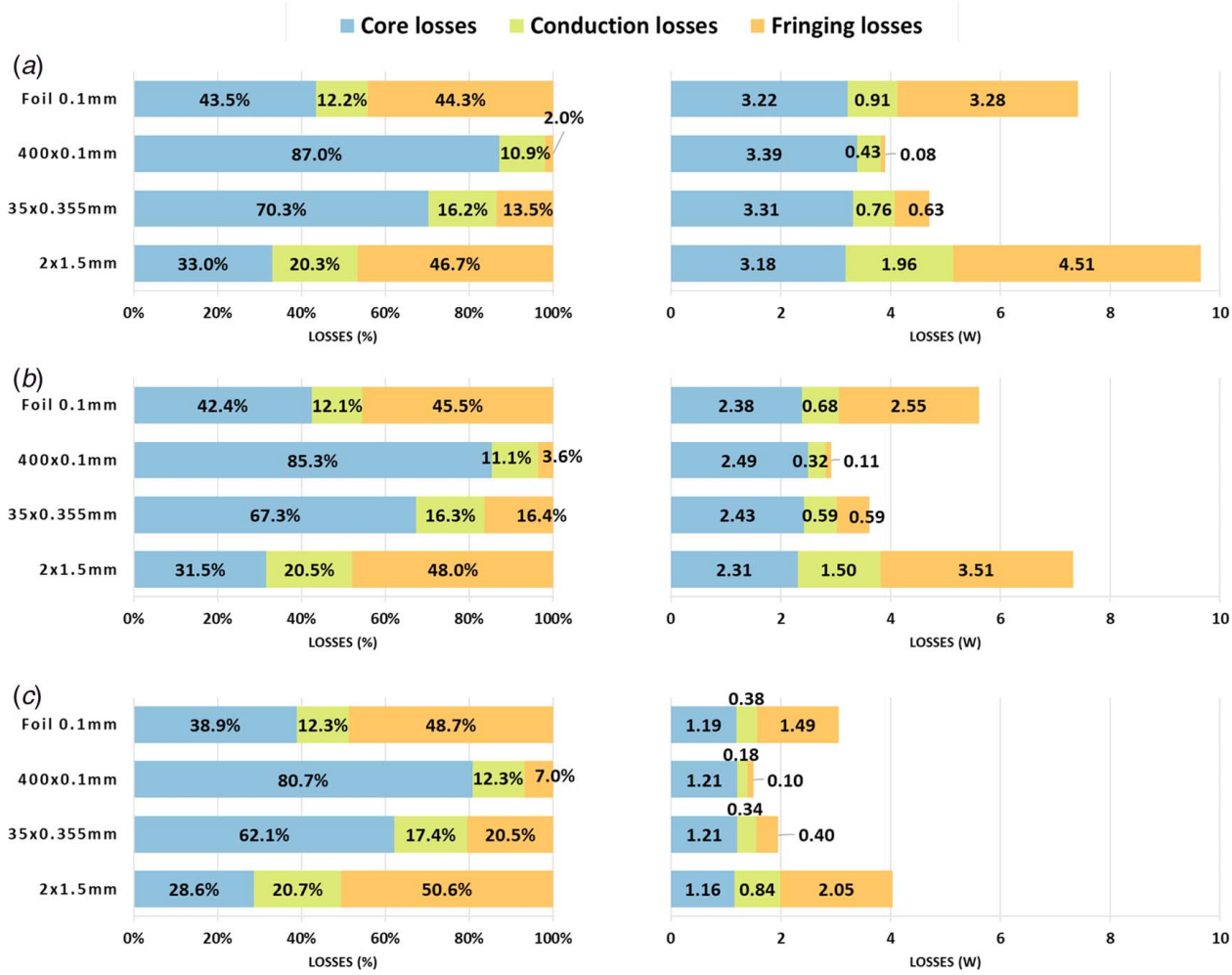

Fig. 6 Decomposed power losses of the inductors for three cases: (*a*) 4A root-mean-square (RMS), (*b*) 3.5A RMS, and (*c*) 2.6A RMS

measurement, the heater used for calibration served as an additional heat source to speed up the heating process to reach steady-state faster. To avoid heating the chamber multiple times, the heater was powered after performing every measurement of an inductor to observe any temperature rise or decrease due to the change of dissipated power and was adjusted accordingly. The current delivered to the heater was such that power losses measured with the power analyzer were similar to confirm the measurement. The way to calculate error has been presented in detail in Ref. [7]. The result of measurement compared to the calibrated calorimetric chamber is presented in Fig. 5. All four inductors with different winding were measured at three different currents of approximate RMS values of 4.0 A, 3.5 A, and 2.6 A. The 4.0 A RMS triangle waveform resulted in approximately 10 W of total losses in 2×1.5 mm winding and heated the chamber to 90 °C. The limiting factor was temperature sensors, which could measure up to 125 °C. Based on calibrated values and using Eqs. (5), (6), (8), and (11), the losses were decomposed into core, conduction and fringing losses as presented in Fig. 6.

Summary

The calorimetric method for estimating low power losses has been presented for inductors. The losses were measured and calculated for chokes, with four different types of winding at three different loads. Although the inductor with Litz wire 400×0.1 mm had the smallest cross-section, it resulted in the smallest amount of conduction losses. Having smaller strands in winding also helps reduce fringing losses, which might consist of a greater portion of total power losses, like with 2×1.5 mm winding, that were at around 50%. The diameter of strands in 35×0.355 mm winding was at the level of skin depth for 35 kHz, and the power losses were an only bit higher compared to 400×0.1 mm winding. This is attributed to the current waveforms' higher-order odd harmonics (3, 5, 7, …) typical for triangular waveforms. The foil winding performs similarly to 2×1.5 mm wire winding, primarily because of the high value of additional losses generated in the copper foil. It can also be seen that core losses were lower for 2×1.5 mm winding, and this is due to the increased temperature, which decreases core losses and has a minimum at around 90 °C [4]. The designer may consider this effect at the designing stage of a particular system to increase overall efficiency.

Acknowledgment

Publication supported by Own Scholarship Fund of the Silesian University of Technology in year 2019/2020.

Conflict of Interest

There are no conflicts of interest.

Nomenclature

A = magnetic vector potential (Wb)
B = magnetic flux density vector (T)
J = current density vector (A/m^2)

V = volume of ferromagnetic core (m^3)
T = period of current waveform (s)
C_2 = ferrite loss thermal coefficient $4.26 \cdot 10^{-6}$ for 3C95 (W/m^3K^2) [4]
C_1 = ferrite loss thermal coefficient $731.8 \cdot 10^{-6}$ for 3C95 (W/m^3K) [4]
C_0 = ferrite loss thermal coefficient $122.7 \cdot 10^{-3}$ for 3C95 (W/m^3) [4]
R_{AC} = AC resistance of winding (Ω)
R_{DC} = DC resistance of winding (Ω)
$R_{th\ outer}$ = thermal resistance of outer chamber walls (K/W)
$R_{th\ inner}$ = thermal resistance of inner chamber walls (K/W)
T_{amb} = ambient temperature (K)
T_{inner} = temperature in inner chamber (K)
T_{ref} = reference temperature 23 (°C)
I_{RMS} = RMS value of current (A)
$k(T)$ = temperature-dependent Steinmetz loss coefficient (W/m^3)
F_R, G_R = skin and proximity effect coefficients
$B(t)$ = absolute value of magnetic flux density at time t (T)
α_{th} = electric resistivity thermal coefficient 0.0039 (1/K)
α, β = Steinmetz loss coefficients $\alpha = 1.045$, $\beta = 2.44$ [4]
δ = skin depth (m)
ΔB = peak-peak value of magnetic flux density (T)
ΔP_{add} = additional total power loss in winding related to skin, proximity, and fringing effects (W)
ΔP_{Cu} = total power loss in winding (W)
ΔP_{Fe} = total power loss in magnetic core (W)
$\Delta P_{tot\ inner}$ = total power loss in inner chamber (inductor and fan) (W)
ΔP_{tot} = total power loss of inductor (W)
ΔP_{out} = total power loss in outer chamber (W)
ΔP_{cond} = total power loss associated with current conduction (W)
ΔP_{fan} = power loss generated by fan (W)
ΔT = temperature rise (K)
ϱ = electrical resistivity (Ωm)
ϱ_{ref} = electrical resistivity at reference temperature T_{ref} (Ωm)
μ_0 = magnetic permeability of vacuum $4 \cdot \pi \cdot 10^{-7}$ (H/m)
μ = magnetic permeability of material (H/m)

References

[1] Kolar, J. W., Krismer, F., Lobsiger, Y., Muhlethaler, J., Nussbaumer, T., and Minibock, J., 2012, "Extreme Efficiency Power Electronics," 2012 7th International Conference on Integrated Power Electronics Systems (CIPS), Nuremberg, Germany, Mar. 6–8, IEEE, pp. 1–22.
[2] Maerz, M., Heckel, T., and Rettner, C., 2015, "Fundamental Efficiency Limits in Power Electronic Systems." 2015 IEEE International Telecommunications Energy Conference (INTELEC), Osaka, Japan, Oct. 18–22, IEEE.
[3] Zámborszky, F., Toth, D., Palanki, Z., and Csizmadia, E., 2014, "Electrical and Calorimetric Power Loss Measurements of Practically Ideal Soft Magnetic Cores," IEEE Trans. Mag., **50**(4), pp. 1–4.
[4] Ferroxcube, "Soft Ferrites and Accessories, Data Handbook," online. https://www.ferroxcube.com/en-global/download/download/11
[5] Micrometals, "Product Catalog," online. www.micrometals.com/
[6] Weier, S., Shafi, M., and Mcmahon, R., 2010, "Precision Calorimetry for the Accurate Measurement of Losses in Power Electronic Devices," IEEE. Trans. Ind. Appl., **46**(1), pp. 278–284.
[7] Christen, D., Badstuebner, U., Biela, J., and Kolar, J., 2010, "Calorimetric Power Loss Measurement for Highly Efficient Converters," The 2010 International Power Electronics Conference – ECCE ASIA, Sapporo, Japan, June 21–24, IEEE, pp. 1438–1445.
[8] Kamei, R., Kim, T.-W., and Kawamura, A., 2011, "Accurate Calorimetric Power Loss Measurement for Efficient Power Converters," The 2010 International Power Electronics Conference–ECCE ASIA, Sapporo, Japan, June 21–24, IEEE.
[9] Malliband, P. D., Carter, D. R. H., Gordon, B. M., and McMahon, R. A., 1998, "Design of a Double-Jacketed, Closed Type Calorimeter for Direct Measurement of Motor Losses," 1998 Seventh International Conference on Power Electronics and Variable Speed Drives (IEEE Conf. Publ. No. 456), London, UK, Sept. 21–23, IET.
[10] Cao, W., Bradley, K., and Ferrah, A., 2009, "Development of a High-Precision Calorimeter for Measuring Power Loss in Electrical Machines," IEEE Trans. Instru. Measur., **58**(3), pp. 570–577.
[11] Itoh, J.-i., and Nigorikawa, A., 2012, "Experimental Analysis on Precise Calorimetric Power Loss Measurement Using Two Chambers," 2012 15th International Power Electronics and Motion Control Conference (EPE/PEMC), Novi Sad, Serbia, Sept. 4–6, IEEE, pp. DS2b.1–1.
[12] Hasegawa, K., and Omura, I., 2018, "Calorimetric Power-Loss Measurement of a High-Power Film Capacitor With Actual Ripple Current Generated by a PWM Inverter," 2018 IEEE Energy Conversion Congress and Exposition (ECCE), Portland, OR, Sept. 23–27, IEEE, pp. 4688–4691.
[13] Venkatachalam, K., Sullivan, C., Abdallah, T., and Tacca, H., 2002, "Accurate Prediction of Ferrite Core Loss With Nonsinusoidal Waveforms Using Only Steinmetz Parameters," 2002 IEEE Workshop on Computers in Power Electronics, 2002. Proceedings., Mayaguez, Puerto Rica, June 3–4, IEEE, pp. 36–41.
[14] Dimitrakakis, G., Tatakis, E., and Rikos, E., 2008, "A Semiempirical Model to Determine Hf Copper Losses in Magnetic Components With Nonlayered Coils," IEEE Trans. Power Elect., **23**(12), pp. 2719–2728.
[15] Krings, A., and Soulard, J., 2010, "Overview and Comparison of Iron Loss Models for Electrical Machines," J. Elect. Eng., **10**(5), pp. 162–169.
[16] Rossmanith, H., Doebroenti, M., Albach, M., and Exner, D., 2011, "Measurement and Characterization of High Frequency Losses in Nonideal Litz Wires," IEEE Trans. Power Elect., **26**(11), pp. 3386–3394.
[17] Greconici, M., Madescu, G., and Moţ, M., 2010, "Skin Effect Analysis in a Free Space Conductor," Facta Univ. Elect. Energ, **23**(1), pp. 207–215.